

Rapid inference for individual binaries and a stochastic background with Pulsar Timing Array data

Aiden Gundersen and Neil J. Cornish
*eXtreme Gravity Institute, Department of Physics,
Montana State University, Bozeman, Montana 59717, USA*

The analysis of pulsar timing array data has provided evidence for a gravitational wave background in the NanoHertz band. This raises the question of what is the source of the signal, is it astrophysical or cosmological in origin? If the signal originates from a population of supermassive black hole binaries, as is generally assumed, we can expect to see evidence for both anisotropy and to be able to resolve signals from individual binaries as more data are collected. The anisotropy and resolvable systems are caused by a small number of loud signals that stand out from the crowd. Here we focus on the joint detection of individual signals and a stochastic background. While methods have previously been developed to perform such an analysis, they are currently held back by the cost of computing the joint likelihood function. Each individual source is described by $N = 8 + 2N_p$ parameters, where N_p are the number of pulsars in the array. With the latest combined data sets having over one hundred pulsars, the parameter space is very large, and consequently, it takes a large number of likelihood evaluations to explore these models. Here we present a new approach that extends the Fourier basis method, previously introduced to accelerate analyses for stochastic signals, to also include deterministic signals. Key elements of the method are that the likelihood evaluations are per-pulsar, avoiding expensive operations on large matrices, and the templates for individual binaries can be computed analytically or using fast Fourier methods on a sparsely sampled grid of time samples. The net result is an analysis that is orders of magnitude faster than previous approaches.

I. INTRODUCTION

Pulsar timing arrays (PTAs) measure the time-of-arrival (TOAs) of radio pulses produced by millisecond pulsars. By recording these TOAs for decades, PTAs are sensitive to gravitational waves (GWs) with nHz frequencies. At the time of writing this paper, evidence for a stochastic gravitational wave background (GWB) has been found by the North American Nanohertz Observatory for Gravitational Waves (NANOGrav), the Parkes Pulsar Timing Array (PPTA), the European Pulsar Timing Array (EPTA), and the Chinese Pulsar Timing Array (CPTA) [1–4]. With this evidence, the next question is: through what process does the GWB signal originate? The most common belief, and one consistent with observed data, is that the background is produced by a population of many supermassive black hole binaries (SMBHBs) in the form of galaxy mergers emitting GWs in the nHz band [1]. However, many cosmological origins for the signal have also been proposed [5, 6]. If the GWB is realized through a population of SMBHBs, then anisotropy in the background and individual binaries should become resolvable as more TOAs are observed [7, 8].

A timing model has been constructed per pulsar that predicts the TOAs to within $\mathcal{O}(1 \mu\text{s})$. The timing model accounts for deterministic delays to the TOAs such as pulsar spin period, spin derivative, pulsar proper motion, and more [9]. The standard timing model does not include models for GW signals, red noise intrinsic to the pulsars, or some sources of white noise such as radiometer noise in the telescopes. These signals not included in the timing model must therefore be modeled jointly in the analysis of PTA data.

Pulsar timing data is unevenly sampled and the noise is heteroscedastic, necessitating the analysis to be carried out in the time-domain. As more TOAs are recorded, the analysis becomes increasingly computationally expensive, by virtue of an expensive likelihood function which must be evaluated many times over the parameter space. The problem is worsened when one considers high-dimensional models with a large parameter volume, increasing the number of likelihood evaluations required.

The likelihood evaluation can be made significantly more efficient by representing the GWB and intrinsic pulsar red noise (RN) in a Fourier basis, as first presented by Lentati et. al. [10]. The Fourier coefficients which describe the signal then become model parameters and must be sampled over, greatly increasing the dimension of the model. The likelihood in this form however is hyper-efficient which could speed up the analysis if the high-dimensional parameter space is explored efficiently.

A general result, that is not widely appreciated, is that for stochastic signals “subtraction equals division” [10–12]. That is, we can either subtract stochastic signals and noise from the data, or instead account for them in the inverse covariance matrix which appears in the likelihood. For stationary stochastic processes it is natural to use a frequency-domain description, and the subtraction can be performed using a basis of sines and cosines. For Gaussian stochastic processes, the amplitudes of the sines and cosines follow a multivariate normal distribution. The amplitudes can be analytically marginalized over (integrated out), resulting in a modified covariance matrix in the marginalized likelihood. This effectively replaces the signal and noise subtraction by division.

In usual PTA analyses, the Fourier coefficients describ-

ing the GWB and RN are analytically marginalized over. This results in a dense covariance matrix which must be inverted for every likelihood evaluation. By including the Fourier coefficients as model parameters and fixing the white noise model, the covariance matrix is constant and its inverse along with relevant inner products can be stored for use in every future likelihood evaluation. There are no expensive matrix inversions in the likelihood when modeling the Fourier coefficients. The drawback to this approach is a high-dimensional model with $\mathcal{O}(10^3)$ model parameters for realistic datasets. It’s therefore crucial that efficient sampling techniques be employed to explore the large parameter volume.

Recently, there has been renewed interest in the Fourier basis approach, with several studies looking at performing what amounts to a “Bayesian Fourier transform”, to first produce posterior distributions for the Fourier coefficients, which can then be used to model the signals and noise in a hierarchical Bayesian analysis [13–15]. Our approach is a little different, in that we apply the signal and noise models concurrently while sampling the Fourier coefficients.

In this paper, we extend the approach from Lentati et al. [10] to include deterministic signals. Generally, the Fourier coefficients can be separated corresponding to the signals they represent: the background, the red noise intrinsic to pulsars, and deterministic signals. As the GWB and RN is a stochastic process, we must include their Fourier coefficients as model parameters and sample over them in the analysis. The TOA-delays induced by deterministic signals however can be evaluated analytically over any choice of time samples, given some set of deterministic model parameters. Then we can represent the deterministic signal with a Fourier basis by either performing an analytic Fourier transform or a discrete fast Fourier transform. We therefore do not need to sample over the Fourier coefficients which represent the deterministic signals. Instead, we sample over the usual deterministic model parameters, and only “under the hood” use its representative Fourier coefficients obtained through a Fourier transform to retain the hyper-efficient likelihood evaluation.

The cost of exploring a model using say, an efficient Markov Chain Monte Carlo (MCMC) algorithm, scales somewhere between linearly and quadratically with the number of parameters. For example, the exploration of posteriors that follow multivariate normal distribution scales quadratically using a naive random-walk Metropolis [16], linearly using ideal Gibbs sampling, and as the five-fourths power using Hamiltonian sampling [17, 18]. The number of parameters in our GWB and RN model scales linearly with the product of the number of pulsars and the number of Fourier coefficients. This number grows as more pulsars are added to the array and as the time span of the dataset increases, necessitating more terms in the Fourier expansion. In contrast, the size of the covariance matrices that appear in the likelihood when the Fourier coefficients are integrated out

grow quadratically with the number of data points, and the cost of inverting these matrices cubically with the number of data points [19]. Then there is the additional cost of sampling the posterior with this expensive likelihood function. The number of data points grows as the product of the number of pulsars and the duration of the observations. In short, our approach scales better than quadratically with the size of the dataset, while the approach currently being used in most PTA analyses scales quartically or worse with the number of data points.

II. CONTINUOUS WAVE SEARCHES

Methods were previously developed to search for one or more individual CW sources, under the simplifying assumption that the correlations induced by a stochastic background could be ignored [20–22]. Later, methods were developed that jointly model the GW background, intrinsic pulsar red noise, and deterministic continuous waves (CWs) from individual SMBHBs [23–25], but these approaches are currently held back by the computational cost. In some of these analyses, the joint model is simplified to make the runtime feasible. For example, if an individual binary has an electromagnetic counterpart, then the parameter space can be reduced in some of its dimensions, say sky location. Presently, NANOGrav and the EPTA have found weak evidence for CWs using various joint analysis techniques [24, 25].

The NANOGrav search for CWs uses a resampling procedure [24]. The analysis was first performed using a common uncorrelated red noise (CURN) and CW model, and the inter-pulsar correlations expected from the GWB were applied in post-processing. Importance weights were calculated using the ratio of likelihoods with and without the inter-pulsar correlations on a thinned set of posterior samples. Sampling according to these weights can produce the posterior for a joint model including GWB correlations. However, relatively few samples survive this process, so the results are not fully robust. The EPTA has also found weak evidence for a CW [25], sampling the likelihood constructed by ENTERPRISE. This likelihood relies on the inversion of dense covariance matrices, and the analysis will not be tractable as the number of observations increases.

QuickCW is a fast analysis for CW + CURN models [22], commonly used in joint analyses. It precomputes and stores filters used in the likelihood for a given set of parameters, and these filters need only be recomputed when a subset of parameters are updated. This leads to a blocked sampling scheme which can efficiently conduct a joint analysis. However, QuickCW does not model inter-pulsar correlations we expect from the GWB. If such correlations were included the filters would have to be recomputed every time the background model parameters were updated. Moreover, the filters in each pulsar would be correlated according to the background. That is, the inner products between filters is no longer diago-

nal in pulsar space, and a dense $4N_p \times 4N_p$ correlation matrix must be computed frequently in the analysis.

In this paper, we present methods which jointly model the background, red noise intrinsic to pulsars, and deterministic signals, such as CWs. This method includes the inter-pulsar correlations expected in the background through hierarchical modeling, so no post-processing is required. Moreover, if the white noise model is fixed, the covariance matrix is as well, and its inverse along with relevant inner products can be precomputed and stored for use in a hyper-efficient likelihood evaluation.

III. SIGNAL MODEL AND LIKELIHOOD

We generalize the signal model from Ref. [10] to include deterministic sources. The extension is fully general, and can be applied to any deterministic signal. The pulse arrival timing data, \mathbf{t} , are made up of contributions from red and white noise, $\mathbf{n}_R, \mathbf{n}_W$, deterministic timing delays \mathbf{t}_T , a stochastic gravitational wave background \mathbf{t}_B , and individual deterministic signals \mathbf{t}_D . The timing residuals are found by subtracting the reference timing model: $\delta\mathbf{t} = \mathbf{t} - \mathbf{t}_T$. The reference timing model is constructed pulsar by pulsar, and does not account for the presence of the gravitational wave signals common to all the pulsars. Because the reference timing model can absorb some of the signals, it is necessary to adjust the timing model when performing a joint analysis of all the data. Under the assumption that the gravitational wave signals produce a small perturbation to the timing model, the correlations are accounted for by linearizing about the reference model:

$$\delta\mathbf{t}' = \delta\mathbf{t} - \mathbf{M}\boldsymbol{\epsilon}, \quad (1)$$

where $\boldsymbol{\epsilon}$ are the linear deviations to the timing model parameters and \mathbf{M} is the timing design matrix [26]. Going one step further and subtracting the signal model and red noise model we are left with the white timing residuals

$$\mathbf{r} = \delta\mathbf{t} - \mathbf{M}\boldsymbol{\epsilon} - \mathbf{t}_B - \mathbf{t}_D - \mathbf{n}_R. \quad (2)$$

Assuming the white noise residuals are Gaussian distributed with zero mean and noise covariance matrix \mathbf{N} , the likelihood function is

$$p(\mathbf{r}|\boldsymbol{\lambda}) = \sqrt{\det((2\pi\mathbf{N})^{-1})} e^{-\frac{1}{2}\mathbf{r}(\boldsymbol{\lambda})^T \mathbf{N}^{-1} \mathbf{r}(\boldsymbol{\lambda})}. \quad (3)$$

Here $\boldsymbol{\lambda}$ denotes all the parameters in the timing model, signal model and red noise model. At this stage, the likelihood can be factored into the product of the likelihoods for each pulsar. Generalizing the treatment of Ref. [10], we express the stochastic background signal, the deterministic signals and the red noise in terms of the Fourier basis \mathbf{F} , with entries

$$F_{kt} = \left\{ \sin\left(\frac{2\pi k}{T}t\right), \cos\left(\frac{2\pi k}{T}t\right) \right\}. \quad (4)$$

The time T is some reference duration that is taken to be equal to or greater than the time span of the longest observed pulsar in the array. The sample times t are different for each pulsar, and are typically unevenly spaced. The discrete frequencies of the Fourier basis are indexed by the integer k . Using this basis we can write

$$\mathbf{t}_B + \mathbf{t}_D + \mathbf{n}_R = \mathbf{F}\mathbf{a} \quad (5)$$

where the coefficients \mathbf{a} have contributions from the three terms:

$$\mathbf{a} = \mathbf{a}_B + \mathbf{a}_D + \mathbf{a}_R. \quad (6)$$

The stochastic components are assumed to be described by zero mean, Gaussian distributions with covariance matrices

$$\begin{aligned} C_{Ii,Jj}^B &= \mathbb{E}[a_{Ii}^B a_{Jj}^B] = \alpha_{IJ} \varphi_i \delta_{ij} \\ C_{Ii,Jj}^R &= \mathbb{E}[a_{Ii}^R a_{Jj}^R] = \delta_{IJ} \kappa_{Ii} \delta_{ij}, \end{aligned} \quad (7)$$

where I, J labels the pulsar and i, j refers to the discrete frequencies. φ_i describe the power spectrum of the stochastic background, and κ_{Ii} denotes the power spectrum of the red noise in the I^{th} pulsar. There is no sum over the repeated indices. The red noise is assumed to be uncorrelated between pulsars, while the stochastic background follows the Hellings-Downs correlation pattern [27]

$$\alpha_{IJ} = \frac{3}{2}\beta_{IJ} \ln \beta_{IJ} - \frac{1}{4}\beta_{IJ} + \frac{1}{2} + \frac{1}{2}\delta_{IJ} \quad (8)$$

where $\beta_{IJ} = (1 - \cos \theta_{IJ})/2$, and θ_{IJ} is the angle between pulsars I and J on the sky. Note that the models assume that the Fourier modes for the stochastic components are orthogonal, which corresponds to assuming the stochastic background and the red noise are stationary. However, because of the uneven sampling in the time-domain, inference of the mode amplitudes will show correlations between different frequencies [10, 28, 29]. In contrast, the coefficients of the deterministic signal model will include correlations between different frequencies. The coefficients are given by

$$\mathbf{a}_D(\boldsymbol{\zeta}) = \mathcal{F}\{\mathbf{h}(\boldsymbol{\zeta})\}, \quad (9)$$

where \mathcal{F} denotes a discrete Fourier transform and $\mathbf{h}(\boldsymbol{\zeta})$ is the time-domain signal, described by parameters $\boldsymbol{\zeta}$. The time-domain signal is sampled on a uniform grid of times $t_m = m\delta t$, with $\delta t = T/N_t$, $N_t = 2k_{\text{max}}$, and k_{max} is the maximum frequency bin used in the analysis. For current day pulsar timing analyses, $k_{\text{max}} = 16$ is sufficient to cover the region where the background and red noise exceed the white noise level (assuming here that $T \sim 20$ yrs). For simple deterministic signals, such as slowly evolving binary black holes, it is possible to compute the discrete Fourier transform analytically. However, the resulting expressions involve trigonometric functions, and

it's sometimes quicker to compute the transform numerically using a fast Fourier transform, depending on the number of Fourier modes modeled.

The complete set of model parameters are then

$$\boldsymbol{\lambda} = \{\boldsymbol{\epsilon}, \boldsymbol{\varphi}, \boldsymbol{\kappa}, \boldsymbol{\zeta}\}. \quad (10)$$

As written, the stochastic components are described by what is called a free spectral model, with no assumption about how the power spectrum varies with frequency. Alternatively, a model for the power spectra can be introduced, such as a power law described by an overall amplitude and spectral index, which can be included as a prior on $\boldsymbol{\varphi}$ and $\boldsymbol{\kappa}$, with the amplitude and spectral index as hyper-parameters.

After specifying priors for the various parameters $\boldsymbol{\lambda}$ the posterior distribution for the model parameters can be found by techniques such as Markov Chain Monte Carlo (MCMC) sampling. However this is not what is usually done since the full parameter space has a very large dimensionality. Instead, by adopting conjugate priors for the parameters $\{\boldsymbol{\epsilon}, \boldsymbol{\varphi}, \boldsymbol{\kappa}\}$ it is possible to analytically marginalize over the Fourier coefficients, resulting in a marginalized likelihood function that depends on far fewer parameters, for example, the amplitude and spectral index of the stochastic background, and the amplitude and spectral index of the red noise in each pulsar. But there is no free lunch. The marginalization results in a new noise covariance matrix \mathbf{K} that depends on a complicated combination of the matrices \mathbf{N} , \mathbf{M} and \mathbf{C} . This dense covariance matrix must be inverted for every likelihood evaluation. Crucially, marginalization over the coefficients of the background \mathbf{a}_B introduces cross terms between pulsars, so the likelihood no longer factors per-pulsar. Recently, efficient GPU based implementations have vastly sped up the otherwise very costly matrix operations that result from the marginalization, but this approach requires a different approach to the sampling to make use of the GPU architecture [30].

In our approach we only analytically marginalize over the timing model, which amounts to replacing \mathbf{N}^{-1} in the likelihood by $\tilde{\mathbf{N}}^{-1} \equiv \mathbf{G}(\mathbf{G}^T \mathbf{N} \mathbf{G})^{-1} \mathbf{G}^T$ where the matrix \mathbf{G} is built from the design matrix \mathbf{M} as in Ref. [26]. Defining the inner product $(\mathbf{u}|\mathbf{v}) = \mathbf{u}^T \tilde{\mathbf{N}}^{-1} \mathbf{v}$, we see that the likelihood involves the terms

$$\begin{aligned} U &= (\delta \mathbf{t} | \delta \mathbf{t}) \\ \mathbf{V}^T &= (\delta \mathbf{t} | \mathbf{F}) \\ \mathbf{W} &= (\mathbf{F} | \mathbf{F}) \end{aligned} \quad (11)$$

where U is a scalar, \mathbf{V} is a vector and \mathbf{W} is a matrix. So long as the white noise model is held fixed these inner products can be computed once and stored. Alternatively, the inner products can be updated periodically if the white noise model is updated in a blocked sampling scheme. The \mathbf{W} matrix would be diagonal if the data were evenly sampled across the full time span T , but the uneven sampling and different time spans lead to off-diagonal terms. However, the matrix is still diagonal

dominant, especially at high frequencies, and most of the off-diagonal terms can be set to zero. The log-likelihood can be written (up to an additive constant) as

$$\begin{aligned} \ln p(\delta \mathbf{t} | \mathbf{a}) &= (\delta \mathbf{t} - \mathbf{F} \mathbf{a})^T \tilde{\mathbf{N}}^{-1} (\delta \mathbf{t} - \mathbf{F} \mathbf{a}) \\ &= -\frac{1}{2} (U - 2 \mathbf{V}^T \mathbf{a} + \mathbf{a}^T \mathbf{W} \mathbf{a}). \end{aligned} \quad (12)$$

The maximum likelihood solution for the Fourier coefficients is then

$$\hat{\mathbf{a}} = \mathbf{W}^{-1} \mathbf{V} \quad (13)$$

and the Fisher information matrix is equal to \mathbf{W} .

A. Individual Black Hole Binaries

The treatment here follows Ref. [31]. Gravitational wave signals can be expressed in terms of the tensor

$$h_{ab}(t, \boldsymbol{\zeta}) = e_{ab}^+(\hat{\Omega}) h_+(t, \boldsymbol{\zeta}) + e_{ab}^\times(\hat{\Omega}) h_\times(t, \boldsymbol{\zeta}), \quad (14)$$

where $\hat{\Omega}$ is a unit vector from the GW source at sky location (θ, ϕ) to the Solar System barycenter (SSB), $h_{+, \times}$ are the polarization amplitudes, and $e_{ab}^{+, \times}$ are the polarization tensors. The polarization tensors can be written in the SSB frame as

$$e_{ab}^+(\hat{\Omega}) = \hat{m}_a \hat{m}_b - \hat{n}_a \hat{n}_b, \quad (15)$$

$$e_{ab}^\times(\hat{\Omega}) = \hat{m}_a \hat{n}_b + \hat{n}_a \hat{m}_b, \quad (16)$$

where

$$\hat{\Omega} = -\sin \theta \cos \phi \hat{x} - \sin \theta \sin \phi \hat{y} - \cos \theta \hat{z}, \quad (17)$$

$$\hat{m} = \sin \phi \hat{x} - \cos \phi \hat{y}, \quad (18)$$

$$\hat{n} = -\cos \theta \cos \phi \hat{x} - \cos \theta \sin \phi \hat{y} + \sin \theta \hat{z}. \quad (19)$$

The response of a pulsar to the source is described by the antenna pattern functions F^+ and F^\times

$$F^+(\hat{\Omega}) = \frac{1}{2} \frac{(\hat{m} \cdot \hat{p})^2 - (\hat{n} \cdot \hat{p})^2}{1 + \hat{\Omega} \cdot \hat{p}}, \quad (20)$$

$$F^\times(\hat{\Omega}) = \frac{(\hat{m} \cdot \hat{p})(\hat{n} \cdot \hat{p})}{1 + \hat{\Omega} \cdot \hat{p}}, \quad (21)$$

where \hat{p} is a unit vector pointing from the Earth to the pulsar. The effect of a GW on a pulsar's residuals can be written as

$$s(t, \boldsymbol{\zeta}) = F^+(\hat{\Omega}) \Delta s_+(t, \boldsymbol{\zeta}) + F^\times(\hat{\Omega}) \Delta s_\times(t, \boldsymbol{\zeta}), \quad (22)$$

where $\Delta s_{+, \times}$ is the difference between the signal induced at the pulsar and at the Earth (the so-called ‘‘pulsar term’’ and ‘‘Earth term’’),

$$\Delta s_{+, \times}(t, \boldsymbol{\zeta}) = s_{+, \times}(t_p, \boldsymbol{\zeta}) - s_{+, \times}(t, \boldsymbol{\zeta}), \quad (23)$$

where t is the time at which the GW passes the SSB and t_p is the time at which it passes the pulsar. From geometry, we can relate t and t_p by

$$t_p = t - L(1 + \hat{\Omega} \cdot \hat{p}), \quad (24)$$

where L is the distance to the pulsar.

For a circular binary, at zeroth post-Newtonian (0-PN) order, $s_{+, \times}$ is given by

$$s_+(t, \zeta) = \frac{\mathcal{M}^{5/3}}{d_L \omega(t)^{1/3}} [\sin 2\Phi(t) (1 + \cos^2 \iota) \cos 2\psi + 2 \cos 2\Phi(t) \cos \iota \sin 2\psi], \quad (25)$$

$$s_\times(t, \zeta) = \frac{\mathcal{M}^{5/3}}{d_L \omega(t)^{1/3}} [-\sin 2\Phi(t) (1 + \cos^2 \iota) \sin 2\psi + 2 \cos 2\Phi(t) \cos \iota \cos 2\psi], \quad (26)$$

where ι is the inclination angle of the SMBHB, ψ is the GW polarization angle, d_L is the luminosity distance to the source, and $\mathcal{M} \equiv (m_1 m_2)^{3/5} / (m_1 + m_2)^{1/5}$ is a combination of the black hole masses m_1 and m_2 called the ‘‘chirp mass.’’ The frequency and phase evolution have the form

$$\omega(t) = \left(\omega_0^{-\frac{8}{3}} - \frac{256}{5} \mathcal{M}^{\frac{5}{3}} t \right)^{-\frac{3}{8}} \quad (27)$$

$$\Phi(t) = \Phi_0 + \frac{1}{32 \mathcal{M}^{5/3}} \left(\omega_0^{-\frac{5}{3}} - \omega^{-\frac{5}{3}} \right)$$

To a good approximation, over the observation time T , the frequency of the Earth term and pulsar term can be taken as constant, however the two frequencies can differ due to the projected time delay:

$$\begin{aligned} \omega_E &= \omega(t_0) \\ \omega_I &= \omega(t_0 - L_I(1 + \hat{\Omega} \cdot \hat{p}_I)) \\ &\approx \omega_E - \frac{96}{5} \omega_E^{11/3} \mathcal{M}^{5/3} L_I(1 + \hat{\Omega} \cdot \hat{p}_I). \end{aligned} \quad (28)$$

This in turn means that the Earth terms and Pulsar terms will have different amplitudes. In principle, the initial phase at each pulsar is fully determined by the sky location, chirp mass and pulsar distance:

$$\begin{aligned} \Phi_I &= \Phi_0 + \frac{1}{32 \mathcal{M}^{5/3}} \left(\omega_0^{-\frac{5}{3}} - \omega_I^{-\frac{5}{3}} \right) \\ &\approx \Phi_0 + (t_0 - L_I(1 + \hat{\Omega} \cdot \hat{p}_I)) \omega_0. \end{aligned} \quad (29)$$

Small changes in the estimate for the pulsar distance, of order a parsec, cause large changes in Φ_I but only small changes in ω_I . Since the Φ_I is only measured modulo 2π , the pulsar distances are in effect only constrained by the frequency measurement. This makes it very difficult to sample the pulsar distance since there are hundreds of local maxima in the likelihood within the envelope of values allowed by frequency measurement. One effective solution is to treat the Φ_I as independent parameters, which takes care of the phase wrapping problem, at the cost of increasing the size of the parameter space.

The full list of parameters for a single binary black hole is then

$$\zeta \rightarrow \{\omega_0, \Phi_0, \mathcal{M}, d_L, \theta, \phi, \iota, \psi, \Phi_I, L_I\}. \quad (30)$$

When there are multiple individual binary signals each has its own set of pulsar phase terms, Φ_I , but they all share the same pulsar distance values L_I .

The full signal $s(t, \zeta)$ in each pulsar can be expressed in terms of constants amplitudes multiplying the functions $\{\cos(\omega_E t), \sin(\omega_E t)\}$, $\{\cos(\omega_I t), \sin(\omega_I t)\}$, the latter being different for each pulsar in the array. For this reason, individual binary signals are often called continuous wave (CW) signals. The discrete Fourier transform (9) can be performed analytically using

$$\begin{aligned} \int_0^T \cos(\omega_k t) \cos(\omega t) dt &= \frac{\sin(\omega T) \omega}{\omega^2 - \omega_k^2} \\ \int_0^T \sin(\omega_k t) \sin(\omega t) dt &= \frac{\sin(\omega T) \omega_k}{\omega^2 - \omega_k^2} \\ \int_0^T \sin(\omega_k t) \cos(\omega t) dt &= \frac{(\cos(\omega T) - 1) \omega_k}{\omega^2 - \omega_k^2} \\ \int_0^T \cos(\omega_k t) \sin(\omega t) dt &= -\frac{(\cos(\omega T) - 1) \omega}{\omega^2 - \omega_k^2}. \end{aligned} \quad (31)$$

These expression can be computed cheaply since they only require two evaluations of trigonometric function, the remaining operations being arithmetic. Moreover, the expressions are highly peaked around $\omega = \omega_k$, so the likelihood can be well approximated using just a few non-zero terms for the \mathbf{a}^D coefficients.

IV. PRIORS AND SAMPLING STRATEGIES

The priors on the red noise coefficients and gravitational wave background coefficients have already been discussed. They take the form of a multi-variate Gaussian distribution with a covariance matrix given by (7). The most straightforward approach is to sample the $N_R = 2N_{p,R} N_f$ red noise coefficients, where $N_{p,R}$ is the number of pulsars which exhibit intrinsic red noise, and the $N_B = 2N_p N_f$ gravitational wave background coefficients directly using what is known as a free spectral model where the amplitudes at each frequency, $\{\varphi_i, \kappa_{Ii}\}$ are allowed to take on any value. A particular spectral model can then be applied in post-processing. Alternatively, the spectral model can be applied as a hyper-prior, with the parameters of the spectral model (e.g. amplitude and spectral index) as hyper-parameters. While it can be more efficient to impose the spectral models directly, the sampling can get trapped in ‘‘Neal’s funnel’’ [32] unless appropriate re-parameterizations are applied [33]. At a given frequency, if the spectrum model has amplitude β_k then prior on the sine and cosine amplitudes $\{a_k^s, a_k^c\}$ each follow a Gaussian distribution with zero mean and variance $\beta_k^2/2$. Alternatively, we

can use a polar parameterization where $a_k^s = A_k \sin \phi_k$, $a_k^c = A_k \cos \phi_k$. The ϕ_k follow a uniform distribution in the range $[0, 2\pi)$, while the scaled amplitudes A_k^2/β_k^2 follow a standard chi-squared distribution with two degrees of freedom. In our current implementation we chose the $\{a_k^s, a_k^c\}$ parameterization.

From here we can analytically marginalize over the red noise coefficients, which reduces the number of parameters that need to be sampled, but at the cost of making the noise covariance matrix more complicated, and the inner products in the likelihood more expensive to compute. Since we need to compute the collection of inner products \mathbf{V} and \mathbf{W} for the background and individual binary models anyway, we keep the red noise coefficients as model parameters and sample them in the analysis. If we were to marginalize over the red noise coefficients, the inner products would have to be recomputed every time the red noise model was updated.

For continuous waves (CWs) originating from individual SMBHBs we use priors that are uniform in $\{\log_{10} \omega_0, \Phi_0, \log_{10} \mathcal{M}, \psi, \cos \iota, \Phi_L\}$ and uniform in space for $\{\log_{10} d_L, \theta, \phi\}$. For the pulsar distances, we use Gaussian priors on L_I , centered on the best estimate found from the dispersion measure (and parallax if available), with a variance estimated from those measurement techniques.

We sample the model parameters using a parallel tempered Markov Chain Monte Carlo (PTMCMC) algorithm. To achieve rapid convergence, we need well-tailored proposal distributions. Some proposals are made with differential evolution [34, 35] to more rapidly resolve correlations in the posterior. Challenges of sampling the high-dimensional parameter space are reduced by studying maximum a posteriori (MAP) solutions. Up to an overall additive constant, the log-posterior is given by

$$\begin{aligned} \ln p(\boldsymbol{\lambda}|\mathbf{d}) = & -\frac{1}{2} \left[U - 2(a_{Ii}^B + a_{Ii}^R + a_{Ii}^D)V_{Ii} \right. \\ & + (a_{Ii}^B + a_{Ii}^R + a_{Ii}^D)(a_{Jj}^B + a_{Jj}^R + a_{Jj}^D)W_{Ii,Jj} \\ & + a_{Ii}^B a_{Jj}^B (C_{Ii,Jj}^B)^{-1} + a_{Ii}^R a_{Jj}^R (C_{Ii,Jj}^R)^{-1} \\ & \left. + \ln \det(2\pi C_{Ii,Jj}^B) + \ln \det(2\pi C_{Ii,Jj}^R) \right]. \end{aligned} \quad (32)$$

The MAP Fourier coefficients $\hat{\mathbf{a}}^R$, $\hat{\mathbf{a}}^B$ are determined by the set of equations $\partial_{a^{(R,B)}} \ln p(\boldsymbol{\lambda}|\mathbf{d})|_{\hat{a}} = 0$:

$$\begin{aligned} -V_{Kk} + (\hat{a}_{Jj}^B + \hat{a}_{Jj}^R + \hat{a}_{Jj}^D)W_{Kk,Jj} + \hat{a}_{Jj}^B (C_{Kk,Jj}^B)^{-1} &= 0 \\ -V_{Kk} + (\hat{a}_{Jj}^B + \hat{a}_{Jj}^R + \hat{a}_{Jj}^D)W_{Kk,Jj} + \hat{a}_{Jj}^R (C_{Kk,Jj}^R)^{-1} &= 0 \end{aligned} \quad (33)$$

Given a set of hyper- and deterministic (CW) model parameters, we can solve the above system to obtain the MAP coefficients, identifying $\hat{\mathbf{a}}^D = \mathcal{F}\{\mathbf{h}(\hat{\boldsymbol{\zeta}})\}$. Then efficient jump proposals in the Fourier coefficients are draws from a multi-variate Gaussian distribution with mean $\hat{\mathbf{a}}$ and covariance matrix $(\mathbf{W} + \mathbf{C}^{-1})^{-1}$ [13].

Another proposal distribution we have found to work well in a range of settings are jumps along eigenvectors of the augmented Fisher information matrix $\boldsymbol{\Sigma}$, with the jump sizes scaled by the inverse square root of the eigenvalues. The augmented Fisher matrix is given by the negative Hessian of second derivatives of the log posterior, meaning that it includes the effects of the priors. For parameters that are well constrained by the likelihood the augmented Fisher matrix is dominated by the contribution from ordinary Fisher matrix, while for parameters that are poorly constrained, using the augmented Fisher matrix is equivalent to making draws from the prior. On its own, the ordinary Fisher matrix is singular due to degeneracies between the a_{Jk}^B and a_{Jk}^R coefficients, but including the priors breaks this degeneracy. The components of the augmented Fisher matrix for the stochastic components are given by

$$\begin{aligned} \Sigma_{a_{Ii}^B, a_{Jj}^B} &= W_{Ii,Jj} + C_{Ii,Jj}^B \\ \Sigma_{a_{Ii}^B, a_{Jj}^R} &= W_{Ii,Jj} \\ \Sigma_{a_{Ii}^R, a_{Jj}^R} &= W_{Ii,Jj} + C_{Ii,Jj}^R. \end{aligned} \quad (34)$$

Using Greek letters to denote the parameters of the deterministic model, the component of the augmented Fisher matrix for the CW has the form

$$\Sigma_{\alpha\beta} = W_{Ii,Jj} \frac{\partial a_{Ii}^D}{\partial \zeta^\alpha} \frac{\partial a_{Jj}^D}{\partial \zeta^\beta} + \delta_{\alpha}^{L_I} \delta_{\beta}^{L_J} \delta_{IJ} \frac{1}{\sigma_{L_I}^2}. \quad (35)$$

In most instances, the terms in the augmented Fisher matrix that involve the pulsar distances are dominated by the contribution from the prior. It is important not to forget the cross terms between the stochastic models and the deterministic model. For example,

$$\Sigma_{\alpha a_{Jj}^B} = W_{Ii,Jj} \frac{\partial a_{Ii}^D}{\partial \zeta^\alpha}. \quad (36)$$

It is possible to represent the CW signal with Fourier coefficients analytically, using sinc functions (31), or numerically with a fast Fourier transform (FFT). In the analysis of simulated data below, we will FFT the CW signal to obtain its Fourier representation. Most of the CW is described by the lowest few frequency bins, so we don't need many sampling points to perform an accurate FFT, making it computationally efficient. Moreover, this approach can be extended to represent arbitrary deterministic signals in the Fourier domain, regardless of whether their analytic Fourier transform is easy to compute. The Fourier representation requires the CW signal to be periodic over the time span of the data, which is generally not true. As a result, Gibbs phenomena [36] appear at either end of the sampling window for the FFT. To remedy this, we extend the sampling window by a few years on both sides, taking time samples before the first pulsar is observed, and after the last pulsar. Generally, we find extending the window by 3 years on either side, for a total of 6 years is sufficient for most datasets. Applying a Tukey window that is flat over the observation

span and tapering to zero in the padded regions further reduces spectral leakage [37]. Because the CW is a deterministic signal, we have the freedom to evaluate it over arbitrary time samples. Then performing a FFT over the extended time span reduces the Gibbs phenomenon and spectral leakage over the time span of the data.

SIMULATED DATASET

We simulate pulsars and TOAs using ENTERPRISE and PTA-REPLICATOR [38, 39]. The dataset contains 15 pulsars with sky locations and distances corresponding to real pulsars observed by NANOGrav. For simplicity, each pulsar in the dataset is observed monthly for 15 years, and the TOA uncertainty is fixed at $0.5 \mu\text{s}$ for every observation. Generally, NANOGrav models three kinds of white noise: EFAC, ECORR, and EQUAD. To simplify the analysis, we used $\text{EFAC} = 1$ for every pulsar in the dataset, and we did not include ECORR nor EQUAD. The white noise model is fixed throughout the analysis.

We inject intrinsic pulsar red noise obeying a power law in 5 of the simulated pulsars. The injected amplitudes and spectral indices which describe the red noise per pulsar are shown in Table I.

pulsar name	$\log_{10} A_{\text{RN}}$	γ_{RN}
J1843-1113	-13.3	0.9
J1024-0719	-13.1	4.1
J1918-0642	-13.5	2.3
J2017+0603	-13.2	5.3
J0636+5128	-13.4	3.3

TABLE I. Pulsars in simulated dataset that include intrinsic red noise with their hyper-parameters: amplitude and spectral index, used for power law signal injection.

We inject a GWB, whose signal is present in every pulsar, according to the hyper-parameters $\log_{10} A_{\text{GWB}} = -14.0$ and $\gamma_{\text{GWB}} = 13/3$. A single deterministic continuous wave (CW) signal with parameters $\omega_0 = 2\pi(4 \times 10^{-9})$, $\Phi_0 = 0$, $\mathcal{M} = 10^{8.35} M_{\odot}$, $d_L = 1.8 \text{Mpc}$, $\theta = \pi/4$, $\phi = \pi/4$, $\iota = \pi/2$, and $\psi = 0$ is also injected. The pulsar distances are set to the parallax distances provided in the NANOGrav dataset, and the pulsar phases are injected according to (29).

The total number of model parameters is $N_m = 2N_f N_p + 2 + 2N_f N_{p,R} + 2N_{p,R} + 2N_p + 8$ where N_f is the number of Fourier modes modeled. In our simulated dataset, we use $N_p = 15$, $N_{p,R} = 5$, and $N_f = 3$ resulting in a total of 170 model parameters. In larger datasets with more pulsars, deterministic sources, and higher frequency resolution, the number of model parameters will be $\mathcal{O}(10^3)$. Although this model is amenable to any arbitrary set of deterministic signals, we inject only one continuous-wave signal into this dataset.

RESULTS

We sample the posterior probability distribution (32) over the model parameters with a PTMCMC algorithm using the sampling techniques discussed above. We use a power law hyper-model (as opposed to a free spectral model) to describe the pulsar intrinsic red noise and the gravitational wave background. That is, we sample over the amplitude and spectral indices which describe these processes, in addition to their Fourier coefficients.

The corner plots for a selection of the model parameters are shown in Figures 1, 3, and 2. Notice that we recover the injected parameters within the spread of the posterior distributions, and the expected correlations (for $f_{\text{ref}} = \text{year}^{-1}$) between the amplitude and spectral index in both the GWB and red noise hyper-models. In Fig. 3, the samples approximately recover the prior as expected.

It can be difficult to model the background and intrinsic red noise per pulsar with so few pulsars. Both signals obey a power law and the GWB is only distinguishable by the Hellings-Downs correlation (8), which is relatively weak. As more pulsars are added to the array, the increase in pulsar pairs improves the detectability of the background.

The correlations between background noise and intrinsic pulsar noise can be seen in Fig. 1. With few pulsars, the GWB and pulsar red noise can fight to describe parts of the data, correlating the sampling. Moreover, the intrinsic red noise in two pulsars can be correlated with one another if both are correlated with the background. There is no physical correlation between the signals injected into the simulated data, but there is correlation in the sampling. This correlation is also illustrated in Fig. 4 where the signal realizations of many samples are plotted. The spread in the background and the intrinsic red noise time-domain signals are wider than their sum, which recovers the residuals.

The results of a free spectral analysis on the simulated data are consistent with the hyper-model as shown in the violin plot, Fig. 5. The free spectral model is identical to the hyper-model, except the power in each frequency bin describing the GWB is allowed to vary freely, as opposed to being constrained to a power law. For the free spectral model, we choose $N_f = 6$ so the power law trend is visible in the violin plot.

FUTURE WORK

The next step is to apply this method to the NANOGrav 15-year dataset. When done properly, this requires us to sample the parameters of the white noise model. This can be accomplished with a blocked sampling scheme, where the white noise model is occasionally updated, and the inner products in the likelihood are recomputed and stored for the next set of sampling. The size of the 15-year dataset will require us to include GPU accelerations developed by other groups when sampling

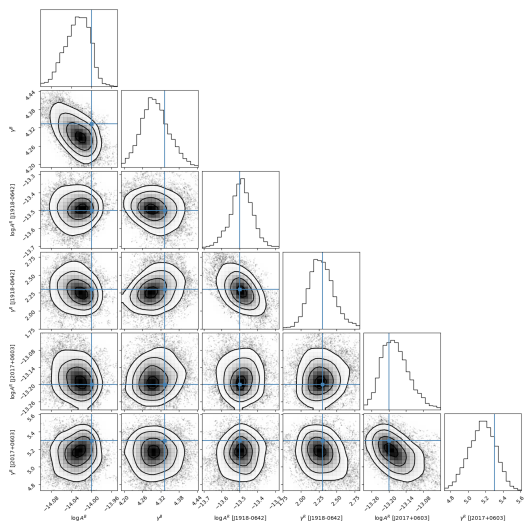


FIG. 1. Samples of selected stochastic hyper-model parameters obtained via MCMC.

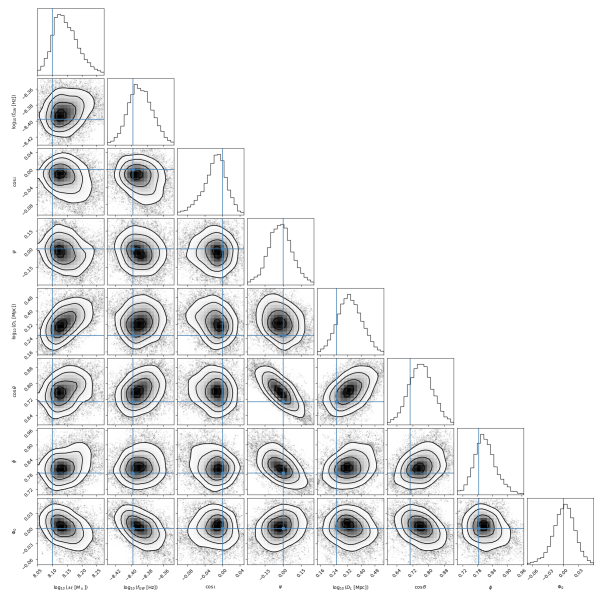


FIG. 2. Samples of continuous wave model parameters obtained via MCMC.

the Fourier coefficients, while enforcing the hyper-prior.

A transdimensional model will also be developed. We have found when N_f is too large, i.e. many Fourier coefficients are modeled, then significant bias is introduced in the parameter estimation. Reversible-jump MCMC (RJMCMC) allow us to sample models with different numbers of Fourier modes, and determine the number of Fourier coefficients favored by the data. A transdi-

dimensional model would also allow for the inclusion of various sets of deterministic signals. For example, RJMCMC could move between models with varying numbers of CW signals [23]. The same techniques used here for CWs can be used to search for other deterministic signals

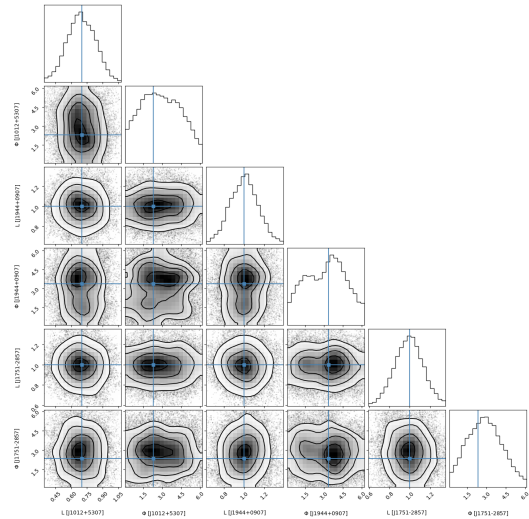


FIG. 3. Samples of selected pulsar distance and initial phase parameters obtained via MCMC.

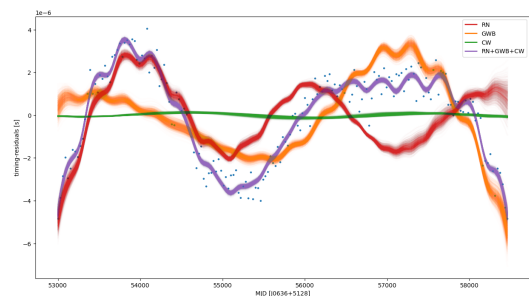


FIG. 4. Bayesogram plotting many time-domain signal realizations from the MCMC samples. Fair draws of intrinsic red noise (RN), gravitational wave background (GWB), continuous wave (CW), and their sum are shown.

such as gravitational wave bursts [40].

We will also look at using our Fourier domain CW model with the per-pulsar Bayesian Fourier transform posteriors described in Ref.[15].

ACKNOWLEDGMENTS

This project was supported by National Science Foundation (NSF) Physics Frontiers Center award 2020265. We thank Bence B'ecsy, Nima Laal, and Rutger van Haasteren for valuable discussions.

[1] G. Agazie, A. Anumalapudi, A. M. Archibald, Z. Arzoumanian, P. T. Baker, B. B'ecsy, L. Blecha, A. Brazier,

P. R. Brook, S. Burke-Spolaor, et al., The Astrophysical

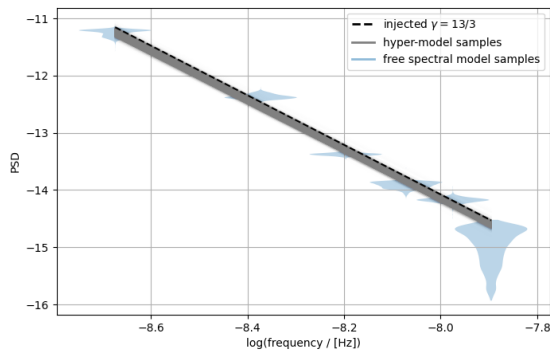


FIG. 5. Violin plot showing results of a free spectral for the gravitational wave background. The power spectral density (PSD) of samples from the power law hyper-model and the injected power law are also plotted.

- Journal Letters **951**, L8 (2023).
- [2] J. Antoniadis, P. Arumugam, S. Arumugam, S. Babak, M. Bagchi, A.-S. B. Nielsen, C. Bassa, A. Bathula, A. Berthreau, M. Bonetti, et al., *Astronomy & Astrophysics* **678**, A50 (2023).
- [3] D. J. Reardon, A. Zic, R. M. Shannon, G. B. Hobbs, M. Bailes, V. Di Marco, A. Kapur, A. F. Rogers, E. Thrane, J. Askew, et al., *The Astrophysical Journal Letters* **951**, L6 (2023).
- [4] H. Xu, S. Chen, Y. Guo, J. Jiang, B. Wang, J. Xu, Z. Xue, R. N. Caballero, J. Yuan, Y. Xu, et al., *Research in Astronomy and Astrophysics* **23**, 075024 (2023).
- [5] A. Afzal et al. (NANOGrav), *Astrophys. J. Lett.* **951**, L11 (2023), [Erratum: *Astrophys. J. Lett.* 971, L27 (2024), Erratum: *Astrophys. J.* 971, L27 (2024)], 2306.16219.
- [6] J. Antoniadis et al. (EPTA, InPTA), *Astron. Astrophys.* **685**, A94 (2024), 2306.16227.
- [7] P. A. Rosado and A. Sesana, *Mon. Not. Roy. Astron. Soc.* **439**, 3986 (2014), 1311.0883.
- [8] B. Bécsy, N. J. Cornish, and L. Z. Kelley, *Astrophys. J.* **941**, 119 (2022), 2207.01607.
- [9] G. Agazie, M. F. Alam, A. Anumrapudi, A. M. Archibald, Z. Arzoumanian, P. T. Baker, L. Blecha, V. Bonidie, A. Brazier, P. R. Brook, et al., *The Astrophysical Journal Letters* **951**, L9 (2023).
- [10] L. Lentati, P. Alexander, M. P. Hobson, S. Taylor, J. Gair, S. T. Balan, and R. van Haasteren, *Phys. Rev. D* **87**, 104021 (2013), 1210.3578.
- [11] N. J. Cornish and J. D. Romano, *Phys. Rev. D* **87**, 122003 (2013), 1305.2934.
- [12] J. D. Romano and N. J. Cornish, *Living Rev. Rel.* **20**, 2 (2017), 1608.06889.
- [13] N. Laal, W. G. Lamb, J. D. Romano, X. Siemens, S. R. Taylor, and R. van Haasteren, *Phys. Rev. D* **108**, 063008 (2023), 2305.12285.
- [14] N. Laal, S. R. Taylor, R. van Haasteren, W. G. Lamb, and X. Siemens (2024), 2410.11944.
- [15] S. Valtolina and R. van Haasteren, *Regularizing the pulsar timing array likelihood: A path towards fourier space*, https://github.com/serevaltolina/PTA_FourierLikelihood (2024).
- [16] A. Gelman, W. R. Gilks, and G. O. Roberts, *The Annals of Applied Probability* **7**, 110 (1997), URL <https://doi.org/10.1214/aoap/1034625254>.
- [17] A. Beskos, N. Pillai, G. Roberts, J.-M. Sanz-Serna, and A. Stuart, *Bernoulli* **19**, 1501 (2013), URL <https://doi.org/10.3150/12-BEJ414>.
- [18] G. E. Freedman, A. D. Johnson, R. van Haasteren, and S. J. Vigeland, *Phys. Rev. D* **107**, 043013 (2023), 2211.01401.
- [19] A. D. Johnson et al. (NANOGrav), *Phys. Rev. D* **109**, 103012 (2024), 2306.16223.
- [20] S. Babak and A. Sesana, *Phys. Rev. D* **85**, 044034 (2012), 1112.1075.
- [21] J. A. Ellis, *Class. Quant. Grav.* **30**, 224004 (2013), 1305.0835.
- [22] B. Bécsy, N. J. Cornish, and M. C. Digman, *Physical Review D* **105**, 122003 (2022).
- [23] B. Bécsy and N. J. Cornish, *Class. Quant. Grav.* **37**, 135011 (2020), 1912.08807.
- [24] G. Agazie, A. Anumrapudi, A. M. Archibald, Z. Arzoumanian, P. T. Baker, B. Bécsy, L. Blecha, A. Brazier, P. R. Brook, S. Burke-Spolaor, et al., *The Astrophysical Journal Letters* **951**, L50 (2023).
- [25] E. Collaboration, I. Collaboration, J. Antoniadis, P. Arumugam, S. Arumugam, S. Babak, M. Bagchi, A.-S. B. Nielsen, C. Bassa, A. Bathula, et al., *A&A* **678**, A50 (2023).
- [26] R. van Haasteren and Y. Levin, *Mon. Not. Roy. Astron. Soc.* **428**, 1147 (2013), 1202.5932.
- [27] R. W. Hellings and G. S. Downs, *Astrophys. J.* **265**, L39 (1983).
- [28] R. van Haasteren and M. Vallisneri, *Mon. Not. Roy. Astron. Soc.* **446**, 1170 (2015), 1407.6710.
- [29] B. Allen and J. D. Romano (2024), 2407.10968.
- [30] M. Vallisneri, M. Crisostomi, A. D. Johnson, and P. M. Meyers, arXiv preprint arXiv:2405.08857 (2024).
- [31] V. Corbin and N. J. Cornish (2010), 1008.1782.
- [32] R. M. Neal, *The annals of statistics* **31**, 705 (2003).
- [33] R. van Haasteren, arXiv preprint arXiv:2406.05081 (2024).
- [34] C. J. T. Braak, *Statistics and Computing* **16**, 239 (2006).
- [35] C. J. Ter Braak and J. A. Vrugt, *Statistics and Computing* **18**, 435 (2008).
- [36] J. W. GIBBS, *Nature* **59**, 606 (1899), URL <https://doi.org/10.1038/059606a0>.
- [37] F. J. Harris, *IEEE Proceedings* **66**, 51 (1978).
- [38] J. A. Ellis, M. Vallisneri, S. R. Taylor, and P. T. Baker, *Astrophysics Source Code Library pp. ascl-1912* (2019).
- [39] B. Bécsy, J. Hazboun, and A. Johnson, *Pta-replicator: Synthesizing simulated pulsar timing array datasets*, https://github.com/bencebecsy/pta_replicator (2024), code adapted from libstempo by Michele Vallisneri.
- [40] B. Bécsy and N. J. Cornish, *Class. Quant. Grav.* **38**, 095012 (2021), 2011.01942.